Injectable, Scalable 3D Tissue-Engineered Model of Marrow Hematopoiesis

Daniel Naveed Tavakol[1]*, Josefine Tratwal[1]*, Fabien Bonini[2]*, Martina Genta[3], Vasco Campos[1], Patrick Burch[4], Sylke Hoehnel[5], Amélie Béduer[2,4], Marco Alessandrini[2], Olaia Naveiras[1, 6]‡ and Thomas Braschler [2]‡

[1]Laboratory of Regenerative Hematopoiesis, Swiss Institute for Experimental Cancer Research & Institute of Bioengineering, Ecole Polytechnique Fédérale de Lausanne (EPFL), Lausanne, Switzerland

[2]Department of Pathology and Immunology, Faculty of Medicine, Université de Genève, Genève, Switzerland

[3]Laboratory of Microsystems Engineering 4, EPFL, Lausanne, Switzerland

[4]Volumina-Medical SA, Route de la Corniche 5, CH-1066 Epalinges, Switzerland

[5]Sun Bioscience, EPFL Innovation Park, Lausanne, Switzerland

[6]Hematology Service, Departments of Oncology and Laboratory Medicine, Centre Hospitalier Universitaire Vaudois (CHUV), Lausanne, Switzerland

These authors contributed equally

‡ Co-Corresponding Authors:
Prof. Olaia Naveiras
Swiss Institute for Experimental Cancer Research (ISREC)
Institute of Bioengineering (IBI)
EPFL
Lausanne, Switzerland 1015

Prof. Thomas Braschler
Faculty of Pathology
University of Genève
Genève, Switzerland

Key Words: Bone marrow niche; Minimally invasive; Stroma; Hematopoietic stem cells; Extramedullary Hematopoiesis; Scaffold

Total Word Count: 8731
Total Figure Count: 6 + 3 Supplementary

ABSTRACT

Modeling the interaction between the supportive stroma and the hematopoietic stem and progenitor cells (HSPC) is of high interest in the regeneration of the bone marrow niche in blood disorders. In this work, we present an injectable co-culture system to study this interaction in a coherent *in vitro* culture and *in vivo* transplantation model. We assemble a 3D hematopoietic niche *in vitro* by co-culture of supportive OP9 mesenchymal cells and HSPCs in porous, chemically defined collagen-coated carboxymethylcellulose microscaffolds (CCMs). Flow cytometry and hematopoietic colony forming assays demonstrate the stromal supportive capacity for *in vitro* hematopoiesis in the absence of exogenous cytokines. After *in vitro* culture, we recover a paste-like living injectable niche biomaterial from CCM co-cultures by controlled, partial dehydration. Cell viability and the association between stroma and HSPCs are maintained in this process. After subcutaneous injection of this living artificial niche *in vivo*, we find maintenance of stromal and hematopoietic populations over 12 weeks in immunodeficient mice. Indeed, vascularization is enhanced in the presence of HSPCs. Our approach provides a minimalistic, scalable, biomimetic *in vitro* model of hematopoiesis in a microcarrier format that preserves the HSPC progenitor function, while being injectable *in-vivo* without disrupting the cell-cell interactions established *in vitro*.

INTRODUCTION:

Hematopoietic stem cells give rise to the entirety of cellular blood components. Clinically, hematopoietic stem and progenitor cell (HSPC) transplantation is routinely used to treat a number of hematological diseases, namely blood cancers such as leukemias and lymphomas, as well as genetic diseases of the blood including severe immune deficiencies and hemoglobinopathies. Successful engraftment of the HSPC transplant in the bone marrow (BM), as well as elimination of residual disease, depends on a multitude of factors, including the BM microenvironment or niche (Derakhshani et al., 2019; Wei and Frenette, 2018). Emergent applications for *in vitro* expansion of HSPCs and models of hematopoiesis for drug testing also critically depend on our understanding of the BM microenvironment. Intense research efforts have been made to recapitulate and analyze the BM niche both *in vitro* and *in vivo* (reviewed in Abarrategi et al., 2018; Bello et al., 2018; Raic et al., 2014; Shih et al., 2017). To date, no standardized model, which is applicable both *in vivo* and *in vitro*, exists. To address this limitation, our study aims to provide a bioengineered system to allow for simple and defined culture of hematopoietic populations, while remaining injectable in a minimally invasive fashion for direct transfer of an *in vitro* niche to an *in vivo* environment.

In vitro models have the advantage of being relatively inexpensive, and therefore provide the opportunity for potentially large screens of therapeutics and disease conditions. Not only have *in vitro* models been used in developing improved hematopoietic expansion protocols (Tajer et al., 2019), but they have also demonstrated great potential for patient-specific drug screening in "organ-on-a-chip" systems (Ronaldson-Bouchard and Vunjak-Novakovic, 2018). Beyond the classical Dexter 2D cultures, more controlled *in vitro* models include bone marrow-on-a-chip PDMS constructs (Sieber et al., 2018; Torisawa et al., 2014), co-cultures of endothelial cells or bone marrow stromal cells (BMSCs) with HSPCs (Butler et al., 2012; Isern et al., 2013; Jing et al., 2010; Li et al., 2007) in polyethylene glycol (PEG) hydrogels (Blache et al., 2016; Raic et al., 2014), collagen membranes or mineralized scaffolds (Lecarpentier et al., 2018; Bourgine et al., 2018). Yet these models are typically not conceived for intact niche transfer *in vivo*, as they require cells to be recovered from cell culture plates or bulky scaffolds.

3D *in vivo* systems are designed to be physiologically more relevant than 2D models. To create and control ectopic BM niches, *in vivo* approaches have typically focused on the induction of mineralized ossicles. Heterotopic bone structures can be generated under the kidney capsule or subcutaneously by direct transplantation of stromal cells or pre-differentiated cartilage pellets (Tavassoli and Crosby, 1968; Friedenstein et al., 1982; Scotti et al., 2013; Serafini et al., 2014), implantation of biomaterials together with growth factors (Shah et al., 2019), or a combination of both cells and biomaterials (Chen et al., 2012; Vaiselbuh et al., 2010). Such *in vivo* models have paved the way for the development of powerful tools for preclinical research or personalized-medicine. Patient-derived xenografts (PDX) models indeed allow for *in vivo* studies of normal or malignant marrow (reviewed in Abarrategi et al., 2018), and provide a platform for physiological

drug screening assays. Major challenges persist in the establishment of PDX marrow models, as ossicles need to be established through rather complex protocols (Reinisch et al., 2017), and expanded via hormonal treatment with daily parathyroid hormone injections for a month or via *in situ* growth factor delivery (Bolander et al., 2016; Shah et al., 2019). To enable minimally invasive delivery of ossicle precursor material, Matrigel has been used as a carrier (Reinisch et al., 2016) with rising concerns over the heterogeneous and batch-dependent composition of this native extracellular matrix-derived material (Hughes et al., 2010).

Here, we develop a harmonized single system for *in vivo* and *in vitro* experiments in the form of a living, injectable hematopoietic niche. To achieve this goal, we have created a co-culture system that allows for a simple, scalable and chemically well-defined microcarrier culture of HSPCs. Concentrated into minimal volumes, this system is also subcutaneously injectable in mice. To mimic the cellular interactions of the hematopoietic niche, the system enables the *in vitro* co-culture of stromal supportive cells and HSPCs in a scalable culture system, as well as a cytokine-free environment, to facilitate *in vitro* screening and possible mass production. During the injection, the system protects the integrity of the cellular payload while maintaining cellular interactions. Finally, *in vivo*, the biomaterial system reconstitutes a porous, mechanically stable structure that over time allows the ingrowth of a vascular and stromal component of host origin to complete the transplanted niche.

Our choice of scaffold is driven by the partial structural and mechanical resemblance of porous hydrogels to trabecular bone, which have been previously shown conductive to *in vitro* (Raic et al., 2014) and *in vivo* (Shah et al., 2019) support for hematopoiesis. Among the various porous scaffolds, compressible scaffolds are of particular interest due to their high mechanical resilience enabling injectability (Bencherif et al., 2012, 2015). Indeed, bulk "BM cryogels" have recently been used as minimally invasive vehicles to generate ossicles *in situ* for enhancement of T cell generation via presentation of the notch ligand DLL-4 (Shah et al., 2019). Here, we develop a cryogel-based, compressible, Collagen-coated Carboxymethyl Microscaffold (CCM). In dilute suspension, these sub-millimetric scaffolds act as microcarriers, enabling scalable cell culture. Yet, thanks to their specific elastic properties, they can be concentrated into a paste-like living biomaterial, prior to minimally invasive implantation by subcutaneous injection. *In vivo*, the microscaffolds interlock to provide a stable, porous implant (Beduer, Bonini, Verheyen et al., manuscript under revision) with a structure reminiscent of trabecular bone.

Our choice of stroma is driven by biological mimicry of the post-natal hematopoietic bone marrow niche. To favor maintenance and expansion of HSPCs in the bone marrow, the importance of various endogenous cell populations has been highlighted, including osteoblasts, endothelial/perivascular cells, and a subset of BMSCs named CXCL12-expressing adventitial reticular (CAR) cells (Bianco, 2014; Calvi et al., 2003; Ding et al., 2012; Sugiyama et al., 2006; Zhang et al., 2003). CAR-like primary BMSCs cells have been shown capable of expanding human

HSPC *in vitro* (Isern et al., 2013), albeit scalability of 3D systems has been limited by HSPC penetrability into the tight spheroids formed by BMSCs cultured in the absence of scaffolds (Schmal et al., 2016). Here we chose to seed our CCM porous scaffolds with the murine, non-clonal BMSC line OP9 (Nakano et al., 1994) to generate a living, injectable stroma supportive for hematopoiesis. The OP9 cell line secretes hematopoietic supportive cytokines *Cxcl12*, *Scf*, and *Angpt1* when co-cultured with HSPCs (Supper et al., 2015) and possesses, in non-clonal assays, the tri-lineage differentiation potential characteristic of BMSCs (Gao et al., 2010), with a particular facility for adipocytic differentiation reminiscent of the recently reported adipoCARs (Baccin et al., 2019). Most importantly, OP9 cells have been shown to provide efficient support of hematopoiesis as compared to other stromal cell lines, probably in large part through paracrine mediated-signaling (Ji et al., 2008; McKinney-Freeman et al., 2008). Indeed, OP9 cells are by themselves sufficient to support hematopoiesis without the need of exogenous cytokines (Naveiras, 2009). This minimal co-culture system reduces interference with *in vitro* screening applications and avoids the difficulty of *in vivo* growth factor delivery (Shah et al., 2019).

Altogether, our approach provides a minimalistic, scalable, biomimetic *in vitro* model of hematopoiesis in a microcarrier format that preserves the HSPC progenitor function in the absence of exogenous cytokines for *in vitro* study, while being injectable for functional *in vivo* readouts, without disrupting the cell-cell interactions established *in vitro*.

METHODS:

Scaffold fabrication

Compressible carboxymethylcellulose scaffolds are produced by cryogel bulk scaffold synthesis, using established protocols with minor modifications. Briefly, a reaction mix consisting of 13.56mg/mL carboxymethylcellulose (AQUALON CMC 7LF PH, 90.5 KDa, DS: 0.84) and 0.486mg/mL adipic acid dihydrazide, buffered with 6.3mg/mL PIPES neutralized to pH 6.7 by 1.2mg/mL NaOH was prepared and filtered through a 0.22um filter (Stericup). After activation by 2.7mg/mL 1-Ethyl-3-(3-dimethylaminopropyl)-carbodiimide (EDC), the mix was frozen at -20°C in 30mL syringes. After 48h of cryo-incubation, the syringes were thawed. The scaffolds thus obtained were then fragmented through a 22G catheter to obtain a suspension of microscaffolds (Beduer, Bonini, Verheyen et al., manuscript under revision). These microscaffolds were then extensively washed, and autoclaved for sterilization.

We express polymer mass, and respectively its concentration, of microscaffold suspensions as dry weight and dry weight per volume. For dry weight determination, microscaffolds contained in a solution or suspension of interest are collected on a 40 µm cell strainer, followed by thorough washing with deionized (DI) water three times, and oven- or microwave-drying of the remaining polymerized material to constant weight (within 1 mg).

Collagen CCMs surface coating

To allow stromal cell (OP9) adhesion, we modified the surface of the sterile microscaffolds with collagen type I (from bovine skin, Sigma, C4243), producing collagen-coated carboxymethylcellulose microscaffolds (CCM). For this, we used a previously published protocol with adaption to the particulate nature of the CCMs (Serex et al., 2018). Briefly, we dehydrated the microscaffolds using a cell strainer in a SteriCup filtration system (C3240). They were washed sequentially with DI water and acetic acid buffer (pH=4, 100 mM). Then, the microscaffolds were immersed in a coating solution containing 10% collagen type I (mass of protein/dry mass of microscaffolds) diluted in acetic acid buffer (pH=4, 10mM). After coating, the collagen-coated carboxymethylcellulose microscaffolds (CCM) were rinsed twice with DI water in order to remove the excess of non-adsorbed proteins. Thereafter, covalent crosslinking of the collagen was performed by immersing the CCMs in a solution containing EDC (1 mg/ml) and MES buffer (pH 4.5, 100 mM) in DI water for 10 minutes. Finally, the CCMs were abundantly rinsed with DI water and a solution of Na_2CO_3 (pH 11, 100 mM) and kept in PBS at 4°C.

Animals

All experimental procedures were approved by the Animal Care and Use Committee of the Canton of Vaud (ACUC, Vaud, Switzerland). All animals were hosted in the EPFL facilities and were kept under a controlled 12 hours light/dark cycle and at constant room temperature 22+/-2°C. DsRed C57BL/6JRj (DsRed) adult male mice were sacrificed and tibiae and femurs were collected for DsRed+ HSPC isolation. 8-16 weeks old NOD SCID-γ (NSG 5557, Jackson laboratories) immunodeficient female mice (n = 3 control; n = 6 experimental) were used as recipients in the transplantation model.

Culture of OP9 stromal cells

Using an established murine mesenchymal stromal cell line (OP9s) (Nakano et al., 1994), cells were expanded at 70-80% confluency for one to two weeks in alpha-minimum essential media (a-MEM) plus Glutamax (32561, ThermoFisher), 10% fetal bovine serum (FBS, 10270-106, GIBCO), and 1% Penicillin/Streptavidin (P/S, 15140122, Thermo Fisher Scientific). OP9 cells were donated from the Daley laboratory (McKinney-Freeman et al., 2009), who received them directly from the Nakano laboratory (Nakano et al., 1994). They were transfected at passage 7-10 with a constitutively expressed GFP lentiviral construct, as specified below, and expanded. Cells were kept at 37˚C and 5% CO_2, and were passaged every 2-4 days at 3:1 or 4:1 ratio, until they reached 70-80% confluency. OP9s were not kept in culture for more than three weeks before use in experiments. Cells were washed with 1x PBS (10010056, Life Technologies) and trypsinized with 0.05% Trypsin-EDTA (25300054 Life technologies), counted, and kept in suspension on ice prior to use.

OP9 stromal cell transfection

Lentiviral particles for GFP introduction were produced by transfecting HEK293T cells using XtremeGene HP transfection reagent with lentiviral packaging plasmid pCMVR8.74 (Addgene #22036), VSV-G envelope expressing plasmid pMD2.G (Addgene #12259) and third-generation transfer vector pRRLSIN.cPPT.PGK-GFP.WPRE (Addgene #12252); all three plasmids were a gift from Didier Trono. Supernatants were collected at 36 and 60 hours post transfection, filtered through 0.22 μm filters and concentrated 1000X using ultracentrifugation. OP9 cells were stably transfected using the concentrated virus titers. Transfected cells were sorted based on GFP expression using FACS after 3 weeks of culture.

Isolation of HSPCs

DsRed adult mice were euthanized with CO_2 according to approved protocols and both tibiae, femurs, and pelvis extracted. After cleaning the bones of all soft tissue, they were kept in PBS on ice until all bones were isolated. Bones from age and gender-matched C57BL/6J wild type controls were isolated in parallel for fluorescence-activated cell sorting (FACS) single-color controls. Bones were subsequently crushed using a mortar and pestle in buffer solution (PBS, 1mM EDTA (15575020, Thermo Fisher Scientific), 2% FBS), until no large chunks of cells were visible. All cell isolation steps were carried out on ice. Cells in suspension and the crushed bones were washed through a 70μm cell strainer and spun down (10 min, 300g, 4˚C). The cell pellets were resuspended in red blood cell lysis buffer (420301, BioLegend) for 30 seconds, before being diluted with buffer solution, and spun down again (5 min, 300g, 4˚C). The cell suspension was stained with a lineage antibody cocktail, washed, and incubated with magnetic beads according to manufacturer's instructions for hematopoietic Lineage depletion (Lin depletion kit : 558451; BD Pharmingen). The total bone marrow cell pellet was resuspended in 3mL volume and loaded into a magnetic separation cell Sorter (AutoMACS, Miltenyi) to remove all lineage positive (Lin+) cells in suspension. The resulting cells were then blocked for 15 minutes on ice (5μg/ml hIgG; I4506-10MG, Sigma Aldrich), and finally stained for one hour on ice with lineage Streptavidin-PO (1/200), as a conjugate to label any remaining Lin+ cells, as well as c-Kit PE-Cy7 (1/200), Sca-1 APC (1/100). After washing the stained cells with buffer solution and straining through a 85μm filter, the cell suspension was run through a FACS system (Aria Fusion) and the resulting Lin-, c-Kit+, and Sca-1+ (KLS) cells were sorted into Iscove's Modified Dulbecco's Medium (IMDM) + Glutamax, 25mM HEPES (31980022, Life Technologies) supplemented with 10% FBS and 1% P/S. In total, 2-3 adult male DsRed+ mice (aged 8-12 weeks) were euthanized to collect approximately 200,000 KLS+ cells in suspension for each experiment. After FACS, cells were kept on ice for approximately 1-2 hours until co-seeding with OP9s on the scaffold.

Co-culture of HSPCs and stromal cells

All cells for co-seeding experiments were cultured in 50% fresh basal media (IMDM + Glutamax 25mM HEPES, 10% FBS, 1% P/S) and 50% conditioned IMDM media (CM). Conditioned media was obtained by culturing confluent GFP+ OP9s with IMDM media for two days (48 hours),

filtering the CM, and freezing the media for no longer than two months at -20˚C. After HSPCs and OP9s were collected in suspension and counted, cells were kept on ice for maximum 1 hour.

3D co-seeding: Collagen-coated microscaffolds (CCMs, 13.5 mg/ml in PBS) were dried using a cell strainer in a SteriCup filtration system (C3240), using an autoclave cloth to transmit the capillary pressure. Once dried, the globule of CCMs was transferred to a 6-well ultra-low adhesion plate (Corning, CLS347) using the tip of a 2 mL stereological pipette. For each condition, the two cell types (HSPCs, OP9s) were combined, spun down, and re-suspended in a minimal amount of media (approximately 100 µL in total). For 2 mg of scaffold per well (dry weight), the following cell ratios were used for the 1:10 "high" seeding (150,000 OP9; 15,000 HSPCs) and 1:100 "low" seeding (150,000 OP9; 1,500 HSPCs). After adding the cell suspension (~100 uL) to the dried scaffold on the ultra-low adhesion plates, the CCMs with cells were incubated for 1 hour at 37˚C and 5% CO_2. After 1 hour, 3 mL of IMDM media (50% conditioned, 50% fresh) was added per well. Co-seeded CCMs were then left in culture for 12 days, with a supplementary dose of 3 mL IMDM media (50% conditioned: 50% fresh basal media) at D7, without removing any of the previous media.

2D co-seeding: OP9 stromal cells were plated on tissue culture-treated plates at a density of 120,000 cells per well in a 6-well plate 1 hour prior to HSPC seeding (~13,000 cells/cm^2), using IMDM media (50% conditioned: 50% fresh). HSPCs were seeded at the previously established co-seeding ratios, 1:10 "high" (12,000 HSPCs per well) and 1:100 "low" (1,200 HSPCs per well). If limited by HSPC cell number, the 2D condition was performed with only the low seeding density. Cells were fed at D7, complementary to the 3D culture timeline, with 3mL added and no media removed, then cultured at 37˚C and 5% CO_2 for 12 days in total. Co-seeding experiments were repeated in at least two separate experiments, with technical triplicates within each experiment.

Compression testing of cells on scaffolds

Compression testing of the HSCP and OP9 loaded CCM scaffold suspensions is described in detail in *Supplement 1*. Briefly, after 3 months of culture with weekly half-media changes, the medium was complemented with Hoechst 33342 (0.1 µg/ml), which stains DNA but also to some extent scaffold filaments due to its cationic nature. The scaffold suspension was then transferred to a compression chamber, for a first viability assessment (see below). This operation resulted in an estimated CCM concentration of 8 +/- 2 mg/mL (supplementary 1). On this suspension, we performed a first linear compression by 75% (10 µm/s compression rate at initial sample heights around 2.5mm). In addition, we performed a second compression by nominally 100% for positive control of cell killing by excessive mechanical forces. We assessed viability by confocal imaging. After every defined set point of compression, 0%, 75%, and 100% respectively, at least five images for every tested sample were taken with a confocal microscope (Zeiss LSM 700 Inverted Confocal Microscope). This procedure was repeated for two independent replicates. The images were analyzed by manually counting OP9 (green), KLS (red) and dead cells (strongly blue nuclei with

loss of both red and green fluorescence). From this, both viability and the ratio of OP9 to KLS within the viable population were determined.

Isolation of cells at D12

Cells were collected for each condition (high/low; 2D/3D) in three fractions: cells in suspension, cells adherent to the CCMs, and any cells adherent to the ultra-low adhesion plates. For cells in suspension, media was collected in a 50 mL falcon tube, and cells were washed and collected twice with serum-free media. For the CCMs adherent fraction, cells were detached via enzymatic digestion as follows. CCMs were transferred to 24 well plates with a 1000 um pipette tip and 1 mL of collagenase I (17100-017, ThermoFisher Scientific) 0.04% was added per well of CCMs for 25 minutes at 37˚C and 5% CO_2. The collagenase digestion was stopped with media complemented with serum, and a stereological pipette was used to dissociate any cells from the CCMs. Finally, cells in solution were run through a 100 µm cell strainer and collected for further manipulation. Trypsin digestion was used for the very limited number of cells adherent to the ultra-low adhesion plates. Cells were spun down and re-suspended in a buffer solution. At this point, each of the conditions (4 total – 2D/3D, High/Low Seeding Density) and each replicate (n = 3 per experiment; two independent experiments) were processed for flow cytometry and for methylcellulose colony forming unit (CFU) assays. Each fraction (non-adherent suspension, collagenase-digested CCM-associated, and bottom-adherent trypsin-digested) was processed separately and the results are presented for all fractions compounded after analysis, based on the total number of cells recovered per well for each of the fractions.

Flow Cytometry

Cell suspensions for each condition and fraction were re-suspended with blocking solution (5µg/ml hIgG) for 10 minutes at room temperature and then Lineage cocktail was added (1:20 dilution) for 20 minutes on ice. After washing with buffer solution and filtered with a 85µm cell strainer, cells were pelleted and re-suspended with antibody mix for 45 minutes on ice. The antibody mix contained: c-Kit (PE-Cy7; 1:200), Sca-1 (BV711; 1:50), CD45 (AF700; 1:100), CD3 (BV421; 1:50), B220 (PE-Cy5; 1:50), CD11b (APC-eFl. 780; 1:1000), and Gr1 (APC; 1:500), diluted in BD Brilliant Stain Buffer (563794, BD Pharmingen). The antibody mix also contained a 1:4 dilution of BrightCount beads (Invitrogen, C36950). Cells were then diluted with DAPI solution (PBS-EDTA and DAPI-UV at 1:5000) and run through a BD LSR II SORP flow cytometer, while resting on ice during the stain preparation.

Methylcellulose CFU Assays

Single cell suspensions, as isolated in 3D (non-adherent, scaffold-adherent, and bottom-adherent) and 2D (non-adherent and bottom-adherent), were separately kept on ice. Each fraction was plated in 1.1ml methylcellulose (M3434, STEMCELL Technologies) in duplicate for each condition and each replicate for hematopoietic clony forming untit /CFU) assay (Mcniece et al., 1990). CD45+ cells were counted with FACS using BrightCount beads (Invitrogen, C36950), to be able to back-

calculate the exact number of cells plated. At Days 7 and 10, each CFU plate was read using a StemVision instrument (Stem Cell Technologies), and total colonies were assessed automatically (StemVision proprietary software) and verified manually on the acquired high-resolution whole-plate images according to colony number, size, and cell distribution (Mcniece et al., 1990).

Subcutaneous Transplantation

After 14 days of *in vitro* culture, seeded-CCMs in suspension were collected from the well plate and poured into the column of the drying device (see video on *Supplementary 2* and detailed description on *Supplementary 3*) allowing for the CCMs to settle down into the reservoir and reach the desired polymer concentration (26 +/- 3 mg/ml, supplementary 3). This condenses the CCMs into a paste-like material with a Young modulus of 1.2+/-0.6 kPa (*Supplementary 1*), which we find sufficient to sustain a 3D architecture *in vivo*. Sterile syringes were used to aspirate 0.1 ml of coated scaffold without cells, followed by 0.1 ml of air to ensure separation between them. The reservoir with the sedimented cultured scaffold (50 µL) was connected to a 1mL syringe and a 20G flexible catheter (BD Biosciences 381703) was plugged in the other end.

NSG mice were chosen for the experiments as OP9 stromal cells are derived from a mixed genetic background and therefore purely syngeneic transplantation was not possible. Prior to injections, anesthesia was induced in NSG mice with 4% isoflurane USP-PPC (Animalcare Ltd). An ophthalmic liquid gel (Viscotears, Alcon) was used to protect the eyes and local isoflurane was reduced to 2%. Mice were placed on a heating pad to keep the temperature constant during intervention, and the back of each mouse was shaved at the area of the injections. Betadine (Mundipharma Medical Company) was spread onto the shaved regions to disinfect the skin.

To perform the subcutaneous injection, a small orifice was created in the disinfected skin using a 18G needle and the 20G catheter (Tro-Vensite i.v. canula, Troge, Hamburg), connected to the loaded syringe, which was gently inserted subcutaneously about 2 cm from the pierced skin (See *Supplement 2*). For each mouse, two separate injections of 50 µL each were performed subcutaneously on either side of the spine. No sutures were required. At the end of the procedure, the mice were placed back in the cage grouped per condition. The entire preparation of the scaffolds and all the injections were performed under the hood to ensure sterility throughout the whole procedure. Each injection, from start to finish, lasted less than 20 minutes per mouse.

Animals were treated with antibiotics in drinking water consisting of 30 mg of Enrofloxacin (300 µL of Baytril 10% ad us. vet, 100 mg/mL, Bayer) and 5 mg of Amoxicillin (100 µL of Amoxi-Mepha 200mg/4mL, Mepha Pharma AG) as well as 500 mg of Paracetamol (Dafalgan®) in a total of 250 mL sterile water for the entire duration of the study and replaced every 7 days. Animals were monitored daily by the researchers, and after two weeks, they were monitored daily by animal care services.

Sacrifice and samples harvesting

NSG immunodeficient mice were euthanized 12 weeks post-injections through inhalation of CO_2 (6 minutes). The back was shaved gently to better localize the two implants. The samples were harvested in each mouse being careful to keep some subcutaneous tissue around to study the integration of the scaffolds within the normal tissue. Samples were then fixed for 24 hours in 4% paraformaldehyde at 4°C (10 mL PFA in 15 mL Falcon tube), washed three times with PBS, and embedded in paraffin.

Histology

Tissues were fixed in paraformaldehyde (PFA), submitted for stepwise dehydration and embedded in paraffin blocks for sectioning at 3-4 µm thickness with a rotary microtome (RM, Leica microsystems). After floating on a water bath to flatten, sections were mounted on glass slides (Superfrost+ slides, Menzel gläser). Paraffin sections were stained with Hematoxylin and eosine (H&E) using the Tissue-Tek Prisma automate (Sakura) and permanently mounted using the Tissue-Tek glas G2-coverslipper (Sakura) to assess morphology. Detection of rabbit anti-GFP (Abcam, ab6673, diluted 1:400), rabbit anti-Dsred (MBL, PM005, diluted 1:500), rat anti-CD31 (clone SZ31, Dianova, DIA-310-M, diluted 1:50), rabbit anti-vWF (Abcam, ab9378, diluted 1:100) or rabbit anti-Perilipin (Abcam, ab3526, diluted 1:200) was performed manually. After quenching with 3% H2O2 in PBS 1x for 10 minutes, a heat pretreatment using 0.1M Tri-Na citrate pH6 was applied at 60°C in a water bath overnight. Primary antibodies were incubated overnight at 4°C. After incubation of a goat, a rat or a rabbit Immpress HRP (Ready to use, Vector Laboratories), revelation was performed with DAB (3,3′-Diaminobenzidine, Sigma-Aldrich). Sections were counterstained with Harris hematoxylin and permanently mounted. Number of CD31+ stained vessels were counted in 2-7 images (500x500µm) covering the entire area of the sectioned scaffold (amounting to 2-7 images per scaffold depending on the size of the scaffold) for four scaffolds each in both the unseeded and seeded conditions.

Microscopy and image quantification

Co-seeded CCMs were kept in 3D culture for 12 days *in vitro*. At days 1, 4, 7, and 11, a small volume of suspended CCMs were removed and transferred to a deep cavity glass microscope slide (produced in lab for imaging, see supplementary 1, Fig. S1-1). Within an hour after transferring CCMs to the imaging chamber, they were imaged at varying magnifications (20X for imaging quantification; 63X for cell morphology) using a Zeiss LSM 700 Inverted Confocal Microscope. As the cells were endogenously labeled for GFP (OP9s) and DsRed (HSPCs), serial imaging was conducted at each time point without significant cellular manipulation. Each image acquired was kept to the same microscope settings as the D0 condition, though as more cells proliferated on the CCMs, laser power was changed to allow for clear image acquisition. In image processing, the ratio of DsRed+ to GFP+ cells was accounted for in order to compare cell proliferation over time. At end point, the seeded CCMs were stained with Hoescht 328 (0.1 µg/ml) to visualize the scaffold filaments themselves.

Images used for quantification were composed of a 25-z-stacked, volume-rendered image. To analyze the data, each fluorescent channel was separated and the compiled volume-rendered image was used. Each image/channel was analyzed using Fiji/ImageJ's threshold tool, with the resulting quantified fluorescent areas converted to cell numbers by using the mean area per cell, as established by manual identification of a subset of the cells. For each 3D experiment, a total of eight independent CCMs were analyzed from two experiments to plot the relative cell proliferation over time.

Statistical Analysis

Values are shown as mean plus or minus the standard deviation (mean +/- SD). Student's t-test was performed for all experiments when comparing two conditions only, or a Two-Way ANOVA for multiple conditions over time. The p-value for statistical significance was $p<0.05$.

RESULTS:

The study aimed to provide a microcarrier co-culture system for convenient and minimally invasive injection of a tissue-like living biomaterial, without disrupting cellular viability and multi-cellular interactions during the injection procedure. We simultaneously seeded stromal OP9s and HSPCs on porous CCM microscaffolds (Figure 1A). The system self-organized such that the OP9 stroma lined the scaffolds coated with collagen I to support the HSPC subpopulations (Figure 1B), and allowed for *in vitro* studies in diluted microcarrier suspension cultures. For subsequent validation *in vivo*, the intact co-cultured CCMs, together with their cellular payload, were dehydrated by a custom dehydration device (Figure 1C, supplementary 3) and delivered *in vivo* by subcutaneous syringe-injection (Figure 1D).

Experimentally, our starting biomaterials are highly elastic and porous microscaffolds consisting of crosslinked carboxymethylcellulose (Beduer, Bonini, Verheyen et al., manuscript under revision). A 3D view based on confocal reconstruction after staining with rhodamine 6G is provided in Figure 1E. The microscaffolds are designed to be reversibly compressible. This allows for facile exchange of the pore fluid by arbitrary sequences of dehydration and rehydration. To obtain the collagen-coated microscaffolds CCM, we made use of such cycles to efficiently and covalently functionalize the microscaffolds with collagen type I to provide native stromal cell adhesion motives.

For the purpose of scaffold seeding, we generated green fluorescent protein (GFP+) OP9 cells and obtained red fluorescent primary murine HSPCs (cKit+Lineage-Sca1+, referred to as KLS) from the marrow of DsRed C57BL/6JRj mice. We then co-seeded a mixture of OP9 stromal cells and KLS+ cells into our CCM scaffolds by making use of the spontaneous aspiration capacity of dehydrated scaffolds to distribute the cells throughout the microscaffolds. *In vitro* culture of this system demonstrated self-organization into a stromal compartment, adopting the scaffold architecture and hosting the HSPCs and their progeny (Figure 1F, Figure 1G).

Collagen-coated, mesenchymal stromal cell-seeded scaffolds promote hematopoietic cell proliferation over time

We first assessed the capacity of the artificial stroma, consisting of CCMs lined with OP9 marrow stromal cells, to support hematopoiesis *in vitro*. We made use of the constitutively expressed fluorescent proteins to allow for the visualization and semi-quantitative analysis of co-cultures by confocal microscopy (Figure 2).

Indeed, confocal imaging showed effective spreading of OP9 stromal cells on the CCM scaffolds and attachment of the co-seeded HSPCs to the OP9s, with continuous proliferation of hematopoietic cells within the scaffold over 11 days in culture (Figure 2A). The stromal cells are essential, since at 24 hours HSPCs failed to adhere to the CCMs in the absence of the OP9 cells (Figure 2B, Figure 2C). In the presence of OP9, we found distinct signs of HSPC supportive characteristics within our *in vitro* hematopoietic niche analog. This included HSPC nestling within OP9 stromal cells (Figure 2D) and colony formation within the matrix after 3-4 days of culture (Figure 2E). Together with the absolute requirement for stromal cells in the absence of exogenous cytokines, this indicated intimate and favorable 3D interactions between the two cell types when loaded into the CCMs.

We then quantified the relative proliferation of the HSPCs in our system. To do so, we seeded the CCMs at two relative HSPC densities: high (1:10) and low (1:100) seeding density (HSPCs to OP9 cells). We followed the relative proliferation of the HSPCs and their progeny by evaluating the area occupied by red fluorescence (DsRed) as compared to green fluorescence (green) in confocal sections of the live co-seeded CCMs over time. By also measuring the average area occupied per HSPC and OP9 (180 μm^2 +/- 90 μm^2 for the HSPC vs. 1270 μm^2 +/- 460 μm^2 for the OP9, n = 8 cells in each case), we converted the area measurements to number ratios of HSPC:OP9. Figure 2F shows that the ratio of HSPCs (and their descendant progenitors) to OP9 cells within the CCMs increased from 0.07+/-0.02 to 1.3+/-0.4 for the high seeding density (intended initial 0.1=1:10 ratio) during 11 days of culture. Likewise, the number ratio HSPCs (and their descendant progenitors) to OP9 increased from 0.018+/-0.01 to 0.12+/-0.03 for the low seeding density (1:100).

This indicated that the seeding density after the initial adhesion step, followed by dilution of the CCMs into a large volume of medium, reflected the original 1:10 and 1:100 ratios. In addition, at both seeding densities, a significant increase in relative numbers of HSPCs and their progeny took place within the CCMs, consistent with effective multiplication and expansion of the HSPCs and their differentiated progeny supported by the OP9 cells in an exogenous cytokine-free environment. However, this microscopic assay underestimated the HSPC multiplication, as numerous cells were observed outside of the CCMs in suspension. Moreover, it does not account for the proliferation of OP9-BMSCs. Due to the constitutive expression of DsRed, it is uninformative regarding the fate of the HSPCs in regards to differentiation or maintenance of stem cell properties, which was thus evaluated through surface protein phenotyping and functional colony assays.

Functional quantification of hematopoietic proliferation on stromal-cell seeded scaffolds as compared to 2D cultures

We next aimed to better characterize the fate of the HSPCs during *in vitro* culture. For this purpose, we used flow cytometry to analyze the co-cultures in 3D on CCMs, and compared them to corresponding standard 2D controls with the same 1:10 and 1:100 initial HSPC:OP9 seeding densities. The constitutive expression of GFP and DsRed by the OP9 cells and HSPCs/progeny, respectively, allowed for the visualization and separation of the OP9 stromal versus the HSPC-derived hematopoietic populations. For example, the dot plot in Figure 3A shows the composition in terms of GFP and DsRed expressing cells for a 3D, 1:10 experiment after 12 days of culture. We found that the HSPCs and their progeny, as identified by the $DsRed^{+}GFP^{-}$ population, consisted nearly exclusively of CD45+ cells, as expected for all cells of the hematopoietic lineage derived from bone marrow HSPCs (Figure 3B) (Weissman and Shizuru, 2008). These cells, which expressed no lineage markers in the cell surface at seeding (Linage- is part of the KLS definition), consisted at day 12 on a mixture of lineage negative and lineage positive cells (Figure 3B). Acquisition of major lineage markers thus revealed hematopoietic differentiation within the CCM coculture. Preservation of c-kit+ expression in a subset of the lineage negative $DsRed^{+}GFP^{-}$CD45+ cells (Figure 3C) suggested the preservation of progenitor function, as later tested in Colony-forming unit (CFU) assays.

Quantitative comparison showed that the total CD45+ cell expansion was significantly higher in 2D 1:10 "high" (254.0±164.4) compared to 3D 1:10 "high" (32.0±13.0, $p=0.0094$) cultures, as well as in 2D 1:100 "low" (530.0±126.3) versus 3D 1:100 "low" (19.0±11.3, $p<0.0001$) cultures (Figure 3D). Very interestingly, although fold expansion of total CD45+ cells was consistently higher in 2D versus 3D conditions, fold expansion of the hematopoietic progenitor compartment as reflected by quantification of phenotypic progenitors ($CD45^{+}Lin^{-}cKit^{+}$ population) was similar for 2D (4.1±3.0) and 3D (2.6±1.2) cultures of the 1:10 "high" seeding density (Figure 3E). Progenitor expansion was higher in 2D versus 3D in the 1:100 condition (4.1±2.7 versus 0.4±0.3, $p=0.0092$). However, total cell recovery from the 3D microscaffolds was challenging to achieve, and thus quantification of hematopoietic expansion may have been underestimated for the 3D conditions, especially for the scarce $CD45^{+}Lin^{-}cKit^{+}$ progenitors in the 1:100 condition, which tightly associate to the stroma to form cobblestone-like colonies.

In order to complete the analysis with functional hematopoietic potency in the co-cultures, we performed CFU assays, which quantify the number of oligopotent progenitors able to form functional hematopoietic clonal colonies after a 7-10 day culture in semi-solid, cytokine-rich media. Like for the FACS analysis, 2D and 3D HSPC/OP9 co-cultures seeded at "low" (1:100) and "high" (1:10) relative HSPC:OP9 ratios were enzymatically digested to obtain a single cell suspension after a 12 day co-culture and plated for CFU assay. Figure 3F shows an example of a CFU assay at 7 days. For the purpose of comparison and to obtain the total number of CFUs produced by each culture condition, CFU counts were normalized per 1000 HSPCs seeded with OP9s at Day 0 (1000 KLS = starting HSPC concentration, $n = 6$ for each condition). The number of CFUs was not significantly different ($p=0.166$ via Two-Way ANOVA) between the 2D and 3D

conditions at each seeding density (1:10 or 1:100, Figure 3G), which is congruent with the CD45+ckit+ hematopoietic progenitor quantification by flow cytometry for the 1:10 "high" density (Figure 3B). The number of relative colonies is significantly higher in the "low" (1:100) seeding condition (2D: 1093.86 ± 567.88, 3D: 764.69 ± 306.84) as compared to the "high" (1:10) condition (2D: 408.34 ± 126.32, 3D: 369.42 ± 99.46), suggestive of either nutrient competition or a negative paracrine regulation by differentiating hematopoietic cells at higher CFU seeding densities. Compared to controls obtained by direct plating of fresh KLS cells without culture prior to the methylcellulose assay, we observed a maintenance, or minor expansion, of the functional HSPC compartment. This is expected and reflects a biomimetic, homeostatic condition, as there is no exogenous addition of any of the cytokines commonly used for *in vitro* HSPC expansion (e.g. thrombopoietin, stem cell factor, or Fms-related tyrosine kinase 3 ligand, (Costa et al., 2018)). The aim here was indeed to provide a minimalistic system enabling further screening without interference from exogeneous cytokines. Overall, we conclude from the *in vitro* functional characterization of our HSPC/OP9 co-cultures that 3D co-culture in CCMs promotes similar expansion of functional hematopoietic progenitors to conventional 2D conditions, with a reduced output of differentiated CD45+Ckit- hematopoietic cells.

Injection of co-seeded CCMs demonstrates both OP9 and donor hematopoiesis in the engineered niche over 12 weeks in vivo in NSG immunodeficient mice

Compressible porous scaffolds have previously demonstrated promise in providing an injectable solution to traditional cell-based tissue engineering techniques (Béduer et al., 2015; Bencherif et al., 2012). In addition to the preservation of hematopoietic progenitor function in the 3D HSPC/OP9 co-culture conditions, we were interested in testing the biocompatibility and hematopoietic support capacity of the HSPC/OP9-loaded CCMs *in vivo*.

Figure 4A-D shows the workflow for transitioning from a microcarrier-like suspension culture to a transplantable co-culture biomaterial. After a predefined time of *in vitro* culture as a dilute suspension (Figure 4A), the CCMs are collected and dehydrated to a controlled level by a device specifically designed for that purpose (Figure 4B, video in Supplementary 2 and detailed information in Supplementary 3). The device applies a pre-set hydrostatic pressure to the CCMs by means of a capillary conductor. As the hydrostatic pressure sustained by the biomaterial constituted by the CCM is strongly linked to its concentration, this ensures constant material consistency compatible with regards to injection and hematopoietic niche reconstitution *in vivo*. Here, we set a hydrostatic pressure difference of 0.2kPa, equivalent to a fluid level difference of about 2cm, to concentrate the co-culture biomaterial to 26 +/- 3 mg/mL (Supplementary 3). At this concentration, the material remains easily injectable and matches the kPa range for the vascular part of the bone marrow niche (Bello et al., 2018), as detailed in Supplementary 3.

After concentration of the co-culture biomaterial, the transfer tip is fitted onto a syringe, and assembled with a catheter (Figure 4C) for subcutaneous injection (Figure 4D). By performing the injection into a cell-culture dish containing medium, we assessed whether the procedure of partial dehydration and passage through the catheter during the injection would be harmful to the

cells (Figure 4E). We found that we are able to retain high viability of cells immediately after injection and 24 hours-post injection, as compared to the pre-injection controls in both the GFP+ OP9s and DsRed+ HSPCs (Figure 4E; $p = 0.822$ via Two-Way ANOVA).

For assessment of the *in vivo* performance of the co-culture biomaterial, we injected the living co-culture biomaterial prepared via the dehydration device into the subcutaneous dorsal region of NSG mice. Supplement 2 includes a video of the entire dehydration and injection procedure. The implants were easily visible externally up to the end of the 12-week follow-up period (Figure 4F). At sacrifice, skin flaps from the back of the animal revealed macroscopic vascularization of the injected scaffolds within the dermal tissue of animals (Figure 4G; Supplement 4).

We carried out two independent sets of experiments to assess the *in vivo* evolution of the co-culture biomaterial. In both sets, the samples consisted of CCMs seeded with HSPCs and OP9s, at the 1:10 initial seeding ratio and cultured for 14 days prior to partial dehydration and implantation. In the first set, we included a control group of scaffolds seeded with OP9 only, whereas in the second set, the control group consisted of completely cell-free CCMs. The aim was to dissect the effect that the scaffold alone, the OP9-seeded scaffolds, or the OP9/HSPC co-seeded scaffolds would have on the *in vivo* outcome. In both sets, after 12 weeks *in vivo*, hematoxylin and eosin (H&E) standard histological staining revealed intact scaffold particles (Figure 5A, D and G). In all conditions, the scaffold was host to diverse cell types. Immunohistochemistry (IHC) against GFP revealed strong persistence of confluent OP9 stroma across the scaffolds shown by the large areas stained in brown (Figure 5E and H). Such staining was absent from the initially cell-free CCM implants (Figure 5B), providing evidence for the specificity of the anti-GFP staining. Similarly, anti-DsRed IHC revealed a positive signal only for scaffolds loaded with both GFP+ OP9s and DsRed+ HSPCs (Figure 5I), indicating persistence of hematopoietic cells from the donor DsRed+ HSPCs 12 weeks after implantation. Lack of DsRed+ signal on scaffolds loaded with only OP9 cells (Figure F) and initially cell-free implants (Figure 5C) attests to the specificity of the anti-DsRed IHC.

The HSPC/OP9-loaded scaffolds macroscopically appeared to vascularize better and conserved a higher proportion of donor-derived stroma (Figure 6F and I) than cell-free scaffolds (Figure 6C). Indeed, HSPC/OP9-seeded scaffolds showed a 6.6 times higher vascularization ($p=0.003$, t-test with Welch approximation after log transform) than cell-free scaffolds, as quantified by relative number of CD31+ vessel segments (Figure 6J).

In the study groups, we observed multinucleated DsRed+ cells, suggesting the presence of specialized donor-derived hematopoietic progeny within the implants, morphologically reminiscent of megakaryocytes, the specialized sessile hematopoietic cells responsible for platelet production. In order to assess megakaryocytic differentiation within the implant, we therefore performed von Willebrand factor (vWF) IHC stains (Fig 6A, D and G). Only HSPC/OP9-seeded scaffolds contained highly positive vWF+ cells (Figure 6D and G), indicative of megakaryocyte lineage commitment within the scaffold, and thus of active *in situ* hematopoiesis. Finally, in order to assess adipocytic differentiation within the implanted scaffolds, we performed IHC stains with

perilipin (Figure 6B, E and H). HSPC/OP9-seeded scaffolds (Figure 6E and H) but not the unseeded controls (Figure 6B), presented frequent areas of adipocyte ghosts with a cytoplasmic perilipin positive signal characteristic of mature adipocytes. In summary, we can conclude from *in vivo* experiments that murine HSPC/OP9-seeded CCM scaffolds can be implanted in NSG mice to produce highly vascularized structures which retain donor stroma and contain locally active hematopoiesis as well as interspersed adipocytes, features reminiscent of adult marrow (Weiss, 1981).

DISCUSSION:

In this study, we developed an easy-to-use system enabling smooth transition from *in vitro* co-culture to an injectable that self-assembles *in situ* to recapitulate structural and mechanical features of the hematopoietic marrow. Its aim was to bridge the gap between various defined co-culture systems *in vitro* and more realistic but complex *in vivo* niches such as long-described heterotopic ossicle formation (Tavassoli and Crosby, 1968; Maniatis et al., 1971; Friedenstein et al., 1982). In orthopedics, porous scaffolds have long been used in conjunction with BM aspirates to enhance bone formation (Yoshii et al., 2009). More recently, they have also been identified as a solution enabling localization of BM niches to a biomaterial, enabling thorough *in vitro* testing of scaffolds prior to implantation, and also targeted implantation (Shah et al., 2019; Shih et al., 2017). Yet, due to the bulk format of these scaffolds, it is difficult to perform live imaging or high-throughput screening on them. We therefore sought to combine the advantages of a microcarrier culture system with the mechanical robustness of a bulk scaffold for hematopoietic niche engineering.

To achieve this goal, we based our system on compressible sub-millimetric carboxymethylcellulose scaffolds. *In vitro*, they can be used as classical microcarrier cultures. Additionally, *in vivo*, these specifically engineered CCM scaffolds self-assemble by microscaffold interlocking (Beduer, Bonini, Verheyen et al., manuscript under revision). The process creates a mechanically stable implant, inducing colonization with a fibrovascular stromal tissue. This dual behavior enables smooth injection of arbitrary scaffold volumes, followed by *in situ* regeneration of a porous niche structurally resembling trabecular bone, with mechanical moduli in the vicinity of 1kPa (measured ex-vivo, supplementary 1), as reported for the vascular niche of the bone marrow (Bello et al., 2018). From a practical point of view, CCMs are easily fabricated with standard equipment (freezer, autoclave for sterilization, laminar flow hood for coating under sterile condition), such that production is easily scalable at affordable cost and compatible with Good Manufacturing Practice (GMP) production.

To enable the adhesion of the stromal OP9 cells, the CCMs feature covalently bound collagen I (Béduer et al., 2018; Serex et al., 2018). Indeed, among a series of extracellular matrix molecules, collagen type I has been shown to provide the highest proliferation levels with KLS cells (Choi and Harley, 2017). Further, contrary to Matrigel used for generation of hematopoietic ossicles (Bello et al., 2018; Hughes et al., 2010; Reinisch et al., 2017), collagen I is a single protein of defined composition that is amenable to clinical use (Lecarpentier et al., 2018; Salvadè et al.,

2007). OP9 cells have been shown to direct pluripotent stem cells towards the hematopoietic fate, and also have an ability to maintain engraftable hematopoietic stem cells in *in vitro* 2D co-cultures systems for up to 2 weeks in the absence of additional cytokines (Naveiras, 2009). In this study, the combination of OP9 cells and CCMs was found not only to enable the baseline culture of HSPCs over 12 days in culture, but also to provide for easy and effective implantation of the hematopoietic scaffolds *in vivo* for a follow-up of 12 weeks in NSG mice.

By stable transfection of OP9 with GFP and the usage of KLS from DsRed mice, the CCMs were readily imaged in 3D culture, and serial imaging gave qualitative insight into early-stage HSPC nestling and cobblestone-like colony formation within the 3D scaffolds. We believe this is indicative of a similar hematopoietic supportive behavior from the stromal cells as compared to 2D controls. We further analyzed the cellular populations phenotypically by flow cytometry, and functionally by CFU assays. We found the output of the 3D cultures, measured as total fold hematopoietic expansion (CD45+), to be lower in 3D than in 2D (Figure 3D). However, the HSPC compartment, as measured by the CFU counts in the 2D versus 3D cultures (Figure 3G), is essentially unaffected by this lower output of total hematopoiesis. As the 3D cultures are effectively concentrated in a much smaller volume with higher local cytokine levels (Rödling et al., 2017), our results point towards differential regulation of hematopoiesis in our configuration leading to HSPC enrichment, which may be ascribed to the difference balance of the hypothesized "vascular" versus "endosteal" niches (Leisten et al., 2012; Sánchez-Aguilera and Méndez-Ferrer, 2017).

Our CCM-based co-culture system was not only amenable to live, high-resolution imaging on sub-samples obtained by simple pipetting, but also allowed for standardized aggregation prior to injection by the use of a specifically designed dehydration device. This avoided loss of cell viability during preparation and injection. At the end of the experiment, the scaffold aggregates were both visible beneath the surface of the mouse's skin and were also easily identifiable with integrated host vasculature after opening of the dermal tissue (Figure 4). Histological staining showed the presence of the GFP+ OP9 with colonies of the DsRed+ HSPC interspersed throughout the recovered tissue sections. Moreover, these implanted CCMs demonstrated no morphologically visible innate inflammatory foreign body response or fibrous capsule surrounding the injected materials. This unique finding supports the hypothesis that homeostatic extramedullary hematopoiesis may be engineered *in vivo* in the form of subcutaneous implants, in the absence of ossification surrounding a marrow cavity, analogous to the soft-tissue masses of benign extramedullary hematopoiesis, often intermixed with adipose tissue, that occur in humans upon extreme hematopoietic demand (Roberts et al., 2016). Previous systems have employed calcified bone surrounding an engineered niche to model hematopoiesis *in vitro* or to encourage hematopoiesis once implanted *in vivo* (Torisawa et al., 2014; Holzapfel et al., 2015; Shafiee et al., 2017; Ventura Ferreira et al., 2016; Blache et al., 2016; Shih et al., 2017; Reinisch et al., 2017; Bourgine et al., 2018). To our knowledge, the system presented here is the first of its kind to show hematopoiesis after long-term *in vivo* subcutaneous transplantation of BMSCs without any calcified bone component.

In this study, we were also cognizant of the multi-cellular complexities associated with BM function, along with recent models incorporating BM adipose tissue *in vitro* (Henriksson et al., 2017; Fairfield et al., 2019). We found mature adipocytes within the scaffolds transplanted with both OP9s and HSPCs, indicating that our model may be of use to study the complex relationships between hematopoiesis and adipocytes *in vitro* and *in vivo* (Mattiucci et al., 2018), a field that has been hampered by the difficulty of immobilizing mature adipocytes in co-culture.

Future work follows the premise of further recapitulating the BM microenvironment by manipulating culture conditions, including addition of hematopoietic cytokines, and the modification of the stromal compartment by replacing the OP9 in the CCMs with a human CAR cell line equivalent for a minimalistic niche, or possibly a mix of cell lines to better reflect the niche heterogeneity. Moreover, by using primary human samples, we may be able to further address the limitations of patient-derived xenograft PDX models (de la Puente et al., 2015; Sánchez-Aguilera and Méndez-Ferrer, 2017; Shah and Singh, 2017; Song et al., 2019). In this respect, our system offers new perspectives for personalized-medicine techniques with the possibility for high-throughput screening *in vitro* followed by validation of selected treatments in a direct implantation *in vivo*.

Conclusion:

In summary, we present in this report a novel 3D co-culture system of HSPCs and BMSCs for studying BM hematopoiesis on chemically defined, collagen-coated cryogel-based scaffold microcarriers. The method for co-seeding two cell populations of the BM is simple and scalable, requiring no exogenous cytokine supplementation for hematopoietic progenitor cell maintenance and proliferation. We further designed a dehydration device enabling on-the-fly preparation of a paste-like injectable implant from dilute suspension cultures. Through minimally invasive subcutaneous transplantation of this living implant, both the stromal and hematopoietic cell populations were able to survive *in vivo* for 12 weeks, showing incorporation into the native tissue via *de novo* vascularization and positive staining for donor GFP+ (OP9 BMSCs) and donor DsRed+ cells (HSPC progeny), including megakaryocytes. Moreover, our tissue engineered BM has provided a first indicator of supporting subcutaneous, extramedullary hematopoiesis in healthy adult murine tissue without simultaneous ossification. We observe some induction of adipogenesis, pointing towards bidirectional communication between the niche and the hematopoietic compartment. A tool allowing to study such bidirectional signaling could be invaluable in both research on PDX models and radiation-induced bone marrow adiposity. In conclusion, this 3D engineering BM niche demonstrates promise to better model the BM microenvironment through a defined *in vitro* to *in vivo* transition, enabling future work in fundamental and patient-specific applications in hematology and bone marrow biology at large.

AUTHOR CONTRIBUTIONS:

O.N. initiated the collaboration. D.N.T., F.B., J.T, M.A., O.N. and T.B. designed the study. P. B., F.B. and T.B. performed biomaterial fabrication. D.N.T., J.T., V.C. and F.B. optimized *in vitro* co-culture conditions. D.N.T and J.T. performed *in vitro* culture and end-point experiments. M.G., D.N.T., F.B., J.T. and A.B. developed the in-vivo injection method. D.N.T. and M.G. performed *in vivo* experiments and J.T. performed end-point analysis. D.N.T., F.B. and J.T. analyzed data and compiled figures. S.H., M.A. and A.B. provided critical insights in biomaterial design and in the overall development of the co-culture system. D.N.T, J.T., F.B., T.B., and O.N. wrote the manuscript. All authors approved of the final form of the manuscript.

ACKNOWELDGEMENTS:

We would like to thank Aurelien Oggier, Dr. Shanti Rojas-Sutterlin and Dr. Philippe Renaud, (EPFL) their input on the experimental design throughout the project. OP9-GFP cells were generated by S.H., V.C. and O.N. while they were members of Prof. Matthias Lutolf's laboratory (EPFL), who kindly donated the cells for the study. The histology data was performed at or with the help of the EPFL Histology Core Facility, notably Dr. Jessica Sordet-Dessimoz. Flow cytometry analysis / cell sorting was performed in the EPFL Flow Cytometry Core Facility. We would also like to thank Thierry Laroche at the EPFL BioImaging & Optics Core Facility (EPFL-BIOP), as well as the Bioimaging Core Facility of the Faculty of Medicine of the University of Geneva for their assistance in training and imaging set up. Further, we thank the caretakers of the EPFL SV animal facilities for their maintenance and support of the long-term animal experiments. Finally, we would like to acknowledge funding sources from the Whitaker International Program (D.N.T), the Anna Fuller Fund (J.T.), the Gebert-Rüf foundation (GRS-043/15 to A.B.), Swiss National Science Foundation (PP00P3_183725 and PP00P3_176990 to O.N.; PP00P2_163684 and PZ00P2_161347 to T.B.).

CONFLICT OF INTEREST STATEMENT:

A. Béduer and T. Braschler declare financial interest in Volumina-Medical SA, Switzerland. P. Burch and A. Béduer are now employees of Volumina-Medical SA. Some of the data in this manuscript has been submitted for a patent application. The other authors declare no conflict of interest.

DATA AVAILABILITY:

The partially processed data required to reproduce these findings are available to download from https://doi.org/10.5281/zenodo.3437654.

REFERENCES:

Abarrategi, A., Mian, S.A., Passaro, D., Rouault-Pierre, K., Grey, W., and Bonnet, D. (2018). Modeling the human bone marrow niche in mice: From host bone marrow engraftment to bioengineering approaches. J. Exp. Med. *215*, 729–743.

Baccin, C., Al-Sabah, J., Velten, L., Helbling, P.M., Grünschläger, F., Hernández-Malmierca, P., Nombela-Arrieta, C., Steinmetz, L.M., Trumpp, A., and Haas, S. (2019). Combined single-cell and spatial transcriptomics reveals the molecular, cellular and spatial bone marrow niche organization. BioRxiv 718395.

Béduer, A., Braschler, T., Peric, O., Fantner, G.E., Mosser, S., Fraering, P.C., Benchérif, S., Mooney, D.J., and Renaud, P. (2015). A compressible scaffold for minimally invasive delivery of large intact neuronal networks. Adv. Healthc. Mater. *4*, 301–312.

Béduer, A., Piacentini, N., Aeberli, L., Da Silva, A., Verheyen, C.A., Bonini, F., Rochat, A., Filippova, A., Serex, L., Renaud, P., et al. (2018). Additive manufacturing of hierarchical injectable scaffolds for tissue engineering. Acta Biomater. *76*, 71–79.

Bello, A.B., Park, H., and Lee, S.-H. (2018). Current approaches in biomaterial-based hematopoietic stem cell niches. Acta Biomater. *72*, 1–15.

Bencherif, S.A., Sands, R.W., Bhatta, D., Arany, P., Verbeke, C.S., Edwards, D.A., and Mooney, D.J. (2012). Injectable preformed scaffolds with shape-memory properties. Proc. Natl. Acad. Sci. U. S. A. *109*, 19590–19595.

Bencherif, S.A., Warren Sands, R., Ali, O.A., Li, W.A., Lewin, S.A., Braschler, T.M., Shih, T.-Y., Verbeke, C.S., Bhatta, D., Dranoff, G., et al. (2015). Injectable cryogel-based whole-cell cancer vaccines. Nat. Commun. *6*, 7556.

Bianco, P. (2014). "Mesenchymal" stem cells. Annu. Rev. Cell Dev. Biol. *30*, 677–704.

Blache, U., Metzger, S., Vallmajo-Martin, Q., Martin, I., Djonov, V., and Ehrbar, M. (2016). Dual Role of Mesenchymal Stem Cells Allows for Microvascularized Bone Tissue-Like Environments in PEG Hydrogels. Adv. Healthc. Mater. *5*, 489–498.

Bolander, J., Ji, W., Geris, L., Bloemen, V., Chai, Y.C., Schrooten, J., and Luyten, F.P. (2016). The combined mechanism of bone morphogenetic protein- and calcium phosphate-induced skeletal tissue formation by human periosteum derived cells. Eur. Cell. Mater. *31*, 11–25.

Bourgine, P.E., Klein, T., Paczulla, A.M., Shimizu, T., Kunz, L., Kokkaliaris, K.D., Coutu, D.L., Lengerke, C., Skoda, R., Schroeder, T., et al. (2018). In vitro biomimetic engineering of a human hematopoietic niche with functional properties. Proc. Natl. Acad. Sci. U. S. A. *115*, E5688–E5695.

Butler, J.M., Gars, E.J., James, D.J., Nolan, D.J., Scandura, J.M., and Rafii, S. (2012). Development of a vascular niche platform for expansion of repopulating human cord blood stem and progenitor cells. Blood *120*, 1344–1347.

Calvi, L.M., Adams, G.B., Weibrecht, K.W., Weber, J.M., Olson, D.P., Knight, M.C., Martin, R.P., Schipani, E., Divieti, P., Bringhurst, F.R., et al. (2003). Osteoblastic cells regulate the haematopoietic stem cell niche. Nature *425*, 841–846.

Chen, Y., Jacamo, R., Shi, Y., Wang, R., Battula, V.L., Konoplev, S., Strunk, D., Hofmann, N.A., Reinisch, A., Konopleva, M., et al. (2012). Human extramedullary bone marrow in mice: a novel in vivo model of genetically controlled hematopoietic microenvironment. Blood *119*, 4971–4980.

Choi, J.S., and Harley, B.A.C. (2017). Marrow-inspired matrix cues rapidly affect early fate decisions of hematopoietic stem and progenitor cells. Sci. Adv. *3*.

Costa, M.H.G., Soure, A.M. de, Cabral, J.M.S., Ferreira, F.C., and Silva, C.L. da (2018). Hematopoietic Niche – Exploring Biomimetic Cues to Improve the Functionality of Hematopoietic Stem/Progenitor Cells. Biotechnol. J. *13*, 1700088.

Derakhshani, M., Abbaszadeh, H., Movassaghpour, A.A., Mehdizadeh, A., Ebrahimi-Warkiani, M., and Yousefi, M. (2019). Strategies for elevating hematopoietic stem cells expansion and engraftment capacity. Life Sci. *232*, 116598.

Ding, L., Saunders, T.L., Enikolopov, G., and Morrison, S.J. (2012). Endothelial and perivascular cells maintain haematopoietic stem cells. Nature *481*, 457–462.

Fairfield, H., Falank, C., Farrell, M., Vary, C., Boucher, J.M., Driscoll, H., Liaw, L., Rosen, C.J., and Reagan, M.R. (2019). Development of a 3D bone marrow adipose tissue model. Bone *118*, 77–88.

Friedenstein, A.J., Latzinik, N.W., Grosheva, A.G., and Gorskaya, U.F. (1982). Marrow microenvironment transfer by heterotopic transplantation of freshly isolated and cultured cells in porous sponges. Exp. Hematol. *10*, 217–227.

Gao, J., Yan, X.-L., Li, R., Liu, Y., He, W., Sun, S., Zhang, Y., Liu, B., Xiong, J., and Mao, N. (2010). Characterization of OP9 as authentic mesenchymal stem cell line. J. Genet. Genomics Yi Chuan Xue Bao *37*, 475–482.

Henriksson, I., Gatenholm, P., and Hägg, D.A. (2017). Increased lipid accumulation and adipogenic gene expression of adipocytes in 3D bioprinted nanocellulose scaffolds. Biofabrication *9*, 015022.

Holzapfel, B.M., Hutmacher, D.W., Nowlan, B., Barbier, V., Thibaudeau, L., Theodoropoulos, C., Hooper, J.D., Loessner, D., Clements, J.A., Russell, P.J., et al. (2015). Tissue engineered humanized bone supports human hematopoiesis in vivo. Biomaterials *61*, 103–114.

Hughes, C.S., Postovit, L.M., and Lajoie, G.A. (2010). Matrigel: a complex protein mixture required for optimal growth of cell culture. Proteomics *10*, 1886–1890.

Isern, J., Martín-Antonio, B., Ghazanfari, R., Martín, A.M., López, J.A., del Toro, R., Sánchez-Aguilera, A., Arranz, L., Martín-Pérez, D., Suárez-Lledó, M., et al. (2013). Self-renewing human

bone marrow mesenspheres promote hematopoietic stem cell expansion. Cell Rep. *3*, 1714–1724.

Ji, J., Vijayaragavan, K., Bosse, M., Menendez, P., Weisel, K., and Bhatia, M. (2008). OP9 stroma augments survival of hematopoietic precursors and progenitors during hematopoietic differentiation from human embryonic stem cells. Stem Cells Dayt. Ohio *26*, 2485–2495.

Jing, D., Fonseca, A.-V., Alakel, N., Fierro, F.A., Muller, K., Bornhauser, M., Ehninger, G., Corbeil, D., and Ordemann, R. (2010). Hematopoietic stem cells in co-culture with mesenchymal stromal cells--modeling the niche compartments in vitro. Haematologica *95*, 542–550.

Lecarpentier, Y., Schussler, O., Sakic, A., Rincon-Garriz, J.M., Soulie, P., Bochaton-Piallat, M.-L., and Kindler, V. (2018). Human Bone Marrow Contains Mesenchymal Stromal Stem Cells That Differentiate In Vitro into Contractile Myofibroblasts Controlling T Lymphocyte Proliferation. Stem Cells Int. *2018*, 6134787.

Leisten, I., Kramann, R., Ventura Ferreira, M.S., Bovi, M., Neuss, S., Ziegler, P., Wagner, W., Knüchel, R., and Schneider, R.K. (2012). 3D co-culture of hematopoietic stem and progenitor cells and mesenchymal stem cells in collagen scaffolds as a model of the hematopoietic niche. Biomaterials *33*, 1736–1747.

Li, N., Feugier, P., Serrurrier, B., Latger-Cannard, V., Lesesve, J.-F., Stoltz, J.-F., and Eljaafari, A. (2007). Human mesenchymal stem cells improve ex vivo expansion of adult human CD34+ peripheral blood progenitor cells and decrease their allostimulatory capacity. Exp. Hematol. *35*, 507–515.

Maniatis, A., Tavassoli, M., and Crosby, W.H. (1971). Origin of osteogenic precursor cells in extramedullary marrow implants. Blood *38*, 569–575.

Mattiucci, D., Naveiras, O., and Poloni, A. (2018). Bone Marrow "Yellow" and "Red" Adipocytes": Good or Bad Cells? Curr. Mol. Biol. Rep. *4*, 117–122.

McKinney-Freeman, S.L., Naveiras, O., and Daley, G.Q. (2008). Isolation of hematopoietic stem cells from mouse embryonic stem cells. Curr. Protoc. Stem Cell Biol. *Chapter 1*, Unit 1F.3.

McKinney-Freeman, S.L., Naveiras, O., Yates, F., Loewer, S., Philitas, M., Curran, M., Park, P.J., and Daley, G.Q. (2009). Surface antigen phenotypes of hematopoietic stem cells from embryos and murine embryonic stem cells. Blood *114*, 268–278.

Mcniece, I.K., Bertoncello, I., Kriegler, A.B., and Quesenberry, P.J. (1990). Colony-forming cells with high proliferative potential (HPP-CFC). Int. J. Cell Cloning *8*, 146–160.

Nakano, T., Kodama, H., and Honjo, T. (1994). Generation of lymphohematopoietic cells from embryonic stem cells in culture. Science *265*, 1098–1101.

Naveiras, O. (2009). Novel determinants of the hematopoietic microenvironment in development and homeostasis - ProQuest. Harvard University.

de la Puente, P., Muz, B., Gilson, R.C., Azab, F., Luderer, M., King, J., Achilefu, S., Vij, R., and Azab, A.K. (2015). 3D tissue-engineered bone marrow as a novel model to study pathophysiology and drug resistance in multiple myeloma. Biomaterials *73*, 70–84.

Raic, A., Rödling, L., Kalbacher, H., and Lee-Thedieck, C. (2014). Biomimetic macroporous PEG hydrogels as 3D scaffolds for the multiplication of human hematopoietic stem and progenitor cells. Biomaterials *35*, 929–940.

Reinisch, A., Thomas, D., Corces, M.R., Zhang, X., Gratzinger, D., Hong, W.-J., Schallmoser, K., Strunk, D., and Majeti, R. (2016). A humanized bone marrow ossicle xenotransplantation model enables improved engraftment of healthy and leukemic human hematopoietic cells. Nat. Med. *22*, 812–821.

Reinisch, A., Hernandez, D.C., Schallmoser, K., and Majeti, R. (2017). Generation and use of a humanized bone-marrow-ossicle niche for hematopoietic xenotransplantation into mice. Nat. Protoc. *12*, 2169–2188.

Roberts, A.S., Shetty, A.S., Mellnick, V.M., Pickhardt, P.J., Bhalla, S., and Menias, C.O. (2016). Extramedullary haematopoiesis: radiological imaging features. Clin. Radiol. *71*, 807–814.

Rödling, L., Schwedhelm, I., Kraus, S., Bieback, K., Hansmann, J., and Lee-Thedieck, C. (2017). 3D models of the hematopoietic stem cell niche under steady-state and active conditions. Sci. Rep. *7*, 4625.

Ronaldson-Bouchard, K., and Vunjak-Novakovic, G. (2018). Organs-on-a-Chip: A Fast Track for Engineered Human Tissues in Drug Development. Cell Stem Cell *22*, 310–324.

Salvadè, A., Belotti, D., Donzelli, E., D'Amico, G., Gaipa, G., Renoldi, G., Carini, F., Baldoni, M., Pogliani, E.M., Tredici, G., et al. (2007). GMP-grade preparation of biomimetic scaffolds with osteo-differentiated autologous mesenchymal stromal cells for the treatment of alveolar bone resorption in periodontal disease. Cytotherapy *9*, 427–438.

Sánchez-Aguilera, A., and Méndez-Ferrer, S. (2017). The hematopoietic stem-cell niche in health and leukemia. Cell. Mol. Life Sci. CMLS *74*, 579–590.

Schmal, O., Seifert, J., Schäffer, T.E., Walter, C.B., Aicher, W.K., and Klein, G. (2016). Hematopoietic Stem and Progenitor Cell Expansion in Contact with Mesenchymal Stromal Cells in a Hanging Drop Model Uncovers Disadvantages of 3D Culture.

Scotti, C., Piccinini, E., Takizawa, H., Todorov, A., Bourgine, P., Papadimitropoulos, A., Barbero, A., Manz, M.G., and Martin, I. (2013). Engineering of a functional bone organ through endochondral ossification. Proc. Natl. Acad. Sci. U. S. A. *110*, 3997–4002.

Serafini, M., Sacchetti, B., Pievani, A., Redaelli, D., Remoli, C., Biondi, A., Riminucci, M., and Bianco, P. (2014). Establishment of bone marrow and hematopoietic niches in vivo by reversion of chondrocyte differentiation of human bone marrow stromal cells. Stem Cell Res. *12*, 659–672.

Serex, L., Braschler, T., Filippova, A., Rochat, A., Béduer, A., Bertsch, A., and Renaud, P. (2018). Pore Size Manipulation in 3D Printed Cryogels Enables Selective Cell Seeding. Adv. Mater. Technol. *3*, 1700340.

Shafiee, A., Baldwin, J.G., Patel, J., Holzapfel, B.M., Fisk, N.M., Khosrotehrani, K., and Hutmacher, D.W. (2017). Fetal Bone Marrow-Derived Mesenchymal Stem/Stromal Cells Enhance Humanization and Bone Formation of BMP7 Loaded Scaffolds. Biotechnol. J. *12*.

Shah, S.B., and Singh, A. (2017). Creating artificial lymphoid tissues to study immunity and hematological malignancies. Curr. Opin. Hematol. *24*, 377–383.

Shah, N.J., Mao, A.S., Shih, T.-Y., Kerr, M.D., Sharda, A., Raimondo, T.M., Weaver, J.C., Vrbanac, V.D., Deruaz, M., Tager, A.M., et al. (2019). An injectable bone marrow-like scaffold enhances T cell immunity after hematopoietic stem cell transplantation. Nat. Biotechnol. *37*, 293–302.

Shih, Y.-R., Kang, H., Rao, V., Chiu, Y.-J., Kwon, S.K., and Varghese, S. (2017). In vivo engineering of bone tissues with hematopoietic functions and mixed chimerism. Proc. Natl. Acad. Sci. U. S. A. *114*, 5419–5424.

Sieber, S., Wirth, L., Cavak, N., Koenigsmark, M., Marx, U., Lauster, R., and Rosowski, M. (2018). Bone marrow-on-a-chip: Long-term culture of human haematopoietic stem cells in a three-dimensional microfluidic environment. J. Tissue Eng. Regen. Med. *12*, 479–489.

Song, Y., Rongvaux, A., Taylor, A., Jiang, T., Tebaldi, T., Balasubramanian, K., Bagale, A., Terzi, Y.K., Gbyli, R., Wang, X., et al. (2019). A highly efficient and faithful MDS patient-derived xenotransplantation model for pre-clinical studies. Nat. Commun. *10*, 366.

Sugiyama, T., Kohara, H., Noda, M., and Nagasawa, T. (2006). Maintenance of the hematopoietic stem cell pool by CXCL12-CXCR4 chemokine signaling in bone marrow stromal cell niches. Immunity *25*, 977–988.

Supper, E., Tahir, S., Imai, T., Inoue, J., and Minato, N. (2015). Modification of Gene Expression, Proliferation, and Function of OP9 Stroma Cells by Bcr-Abl-Expressing Leukemia Cells. PLOS ONE *10*, e0134026.

Tajer, P., Pike-Overzet, K., Arias, S., Havenga, M., and Staal, F.J.T. (2019). Ex Vivo Expansion of Hematopoietic Stem Cells for Therapeutic Purposes: Lessons from Development and the Niche. Cells *8*, 169.

Tavassoli, M., and Crosby, W.H. (1968). Transplantation of marrow to extramedullary sites. Science *161*, 54–56.

Torisawa, Y., Spina, C.S., Mammoto, T., Mammoto, A., Weaver, J.C., Tat, T., Collins, J.J., and Ingber, D.E. (2014). Bone marrow-on-a-chip replicates hematopoietic niche physiology in vitro. Nat. Methods *11*, 663–669.

Vaiselbuh, S.R., Edelman, M., Lipton, J.M., and Liu, J.M. (2010). Ectopic human mesenchymal stem cell-coated scaffolds in NOD/SCID mice: an in vivo model of the leukemia niche. Tissue Eng. Part C Methods *16*, 1523–1531.

Ventura Ferreira, M.S., Bergmann, C., Bodensiek, I., Peukert, K., Abert, J., Kramann, R., Kachel, P., Rath, B., Rütten, S., Knuchel, R., et al. (2016). An engineered multicomponent bone marrow niche for the recapitulation of hematopoiesis at ectopic transplantation sites. J. Hematol. Oncol.J Hematol Oncol *9*, 4.

Wei, Q., and Frenette, P.S. (2018). Niches for Hematopoietic Stem Cells and Their Progeny. Immunity *48*, 632–648.

Weiss, L. (1981). Haemopoiesis in Mammalian Bone Marrow. In Ciba Foundation Symposium 84 - Microenvironments in Haemopoietic and Lymphoid Differentiation, (Wiley-Blackwell), pp. 5–21.

Weissman, I.L., and Shizuru, J.A. (2008). The origins of the identification and isolation of hematopoietic stem cells, and their capability to induce donor-specific transplantation tolerance and treat autoimmune diseases. Blood *112*, 3543–3553.

Yoshii, T., Sotome, S., Torigoe, I., Tsuchiya, A., Maehara, H., Ichinose, S., and Shinomiya, K. (2009). Fresh bone marrow introduction into porous scaffolds using a simple low-pressure loading method for effective osteogenesis in a rabbit model. J. Orthop. Res. Off. Publ. Orthop. Res. Soc. *27*, 1–7.

Zhang, J., Niu, C., Ye, L., Huang, H., He, X., Tong, W.-G., Ross, J., Haug, J., Johnson, T., Feng, J.Q., et al. (2003). Identification of the haematopoietic stem cell niche and control of the niche size. Nature *425*, 836–841.

FIGURES:

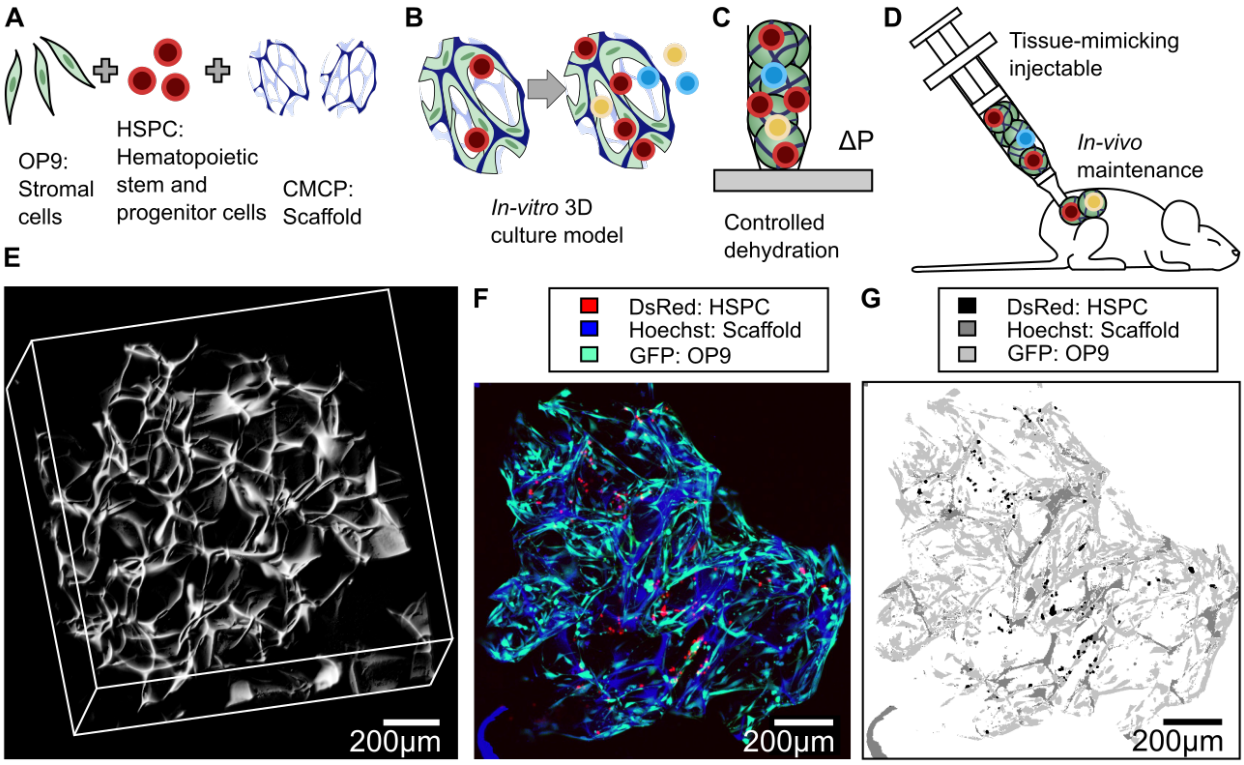

Figure 1. Transplantable bone marrow niche.

A) For in vitro culture, stromal cells (OP9) are combined with hematopoietic stem and progenitor cells (HSPC, selected from bone marrow as lineage-, ckit+, Sca-1+ cells); the resulting cell mix is loaded onto collagen-coated carboxymethylcellulose microparticles (CCMs). **B)** During in-vitro culture, the stromal cells adhere to the scaffold and at the same time provide support to the proliferating and differentiating HSPC. **C)** For in-vivo implantation, the cell-loaded CCMs are slowly dehydrated to form a paste-like implantable living biomaterial. Both dehydration speed and final dehydration level are carefully controlled. **D)** The resulting tissue-mimicking biomaterial is injected subcutaneously for in vivo follow-up. **E)** Structure of a CCM. **F)** CCM (stained by cell impermeant Hoechst dye) along with green fluorescent stroma and red fluorescent hematopoietic compartment. **G)** Assignment of the different areas as scaffold, HSPCs and lineage-committed progenitors, and stromal cells (OP-9). Confocal images are linearly contrast adjusted.

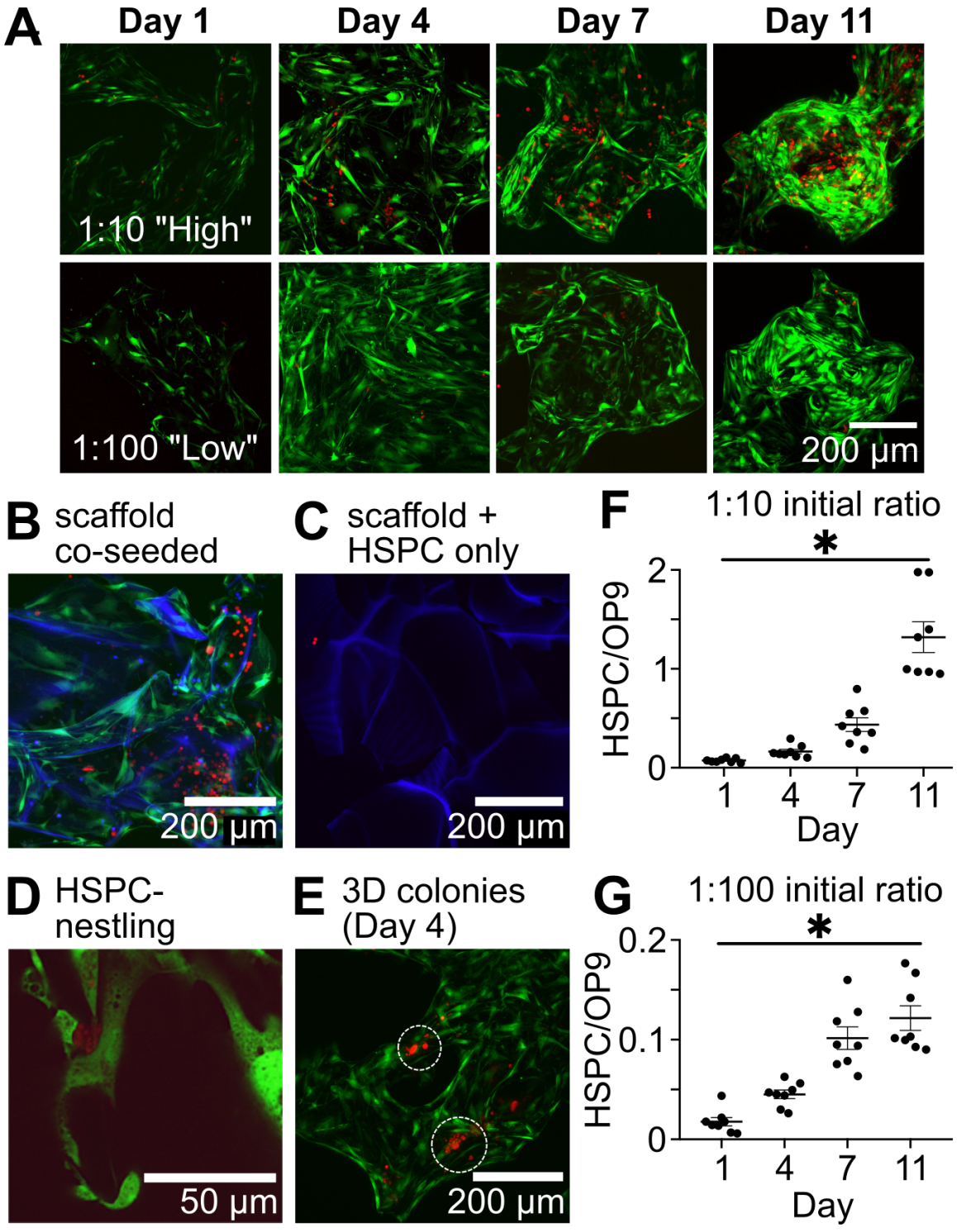

Fig. 2. In-vitro co-culture of OP9 MSCs and HSPCs on CCMs.

(A) Serial confocal imaging qualitatively demonstrates an increase in hematopoietic populations over the span of nearly two weeks in co-culture, for both 1:10 and 1:100 seeding densities (HSPC:MSC); green = GFP+ OP9 MSCs, red = DsRed+ HSPCs; scale

bar = 100 um. Qualitative observations from imaging demonstrate large-scale structural outline of the seeded CCMs. **(B)** scale bar = 200 um. DsRed+ HSPCs requiring MSCs to attach and proliferate (scale bar = 100 um), very few DsRed+ cells are found at 24h with OP9 support. **(C-E)** focal imaging of co-seeded scaffolds at higher magnification showing HSPCs nestling within the MSC feeder layers (**D**, scale bar = 200 um), and 3D colonies (**E**), appearing throughout the scaffolds over as short as four days in culture (scale bar = 50-500 um, indicated on image). Note that in the absence of OP9 stroma **(C)** HSCPs are not retrieved within the scaffold at day 4 **(F-G)** Quantification of proliferation ratios for HSPC to OP9 in co-seeded scaffolds from confocal image z-stacks (**F** for 1:10 seeding ratio, **G** for 1:100 seeding ratio, 25 total images per "n"; n = 8 per condition, total of 200 slices). Confocal images are linearly contrast adjusted.

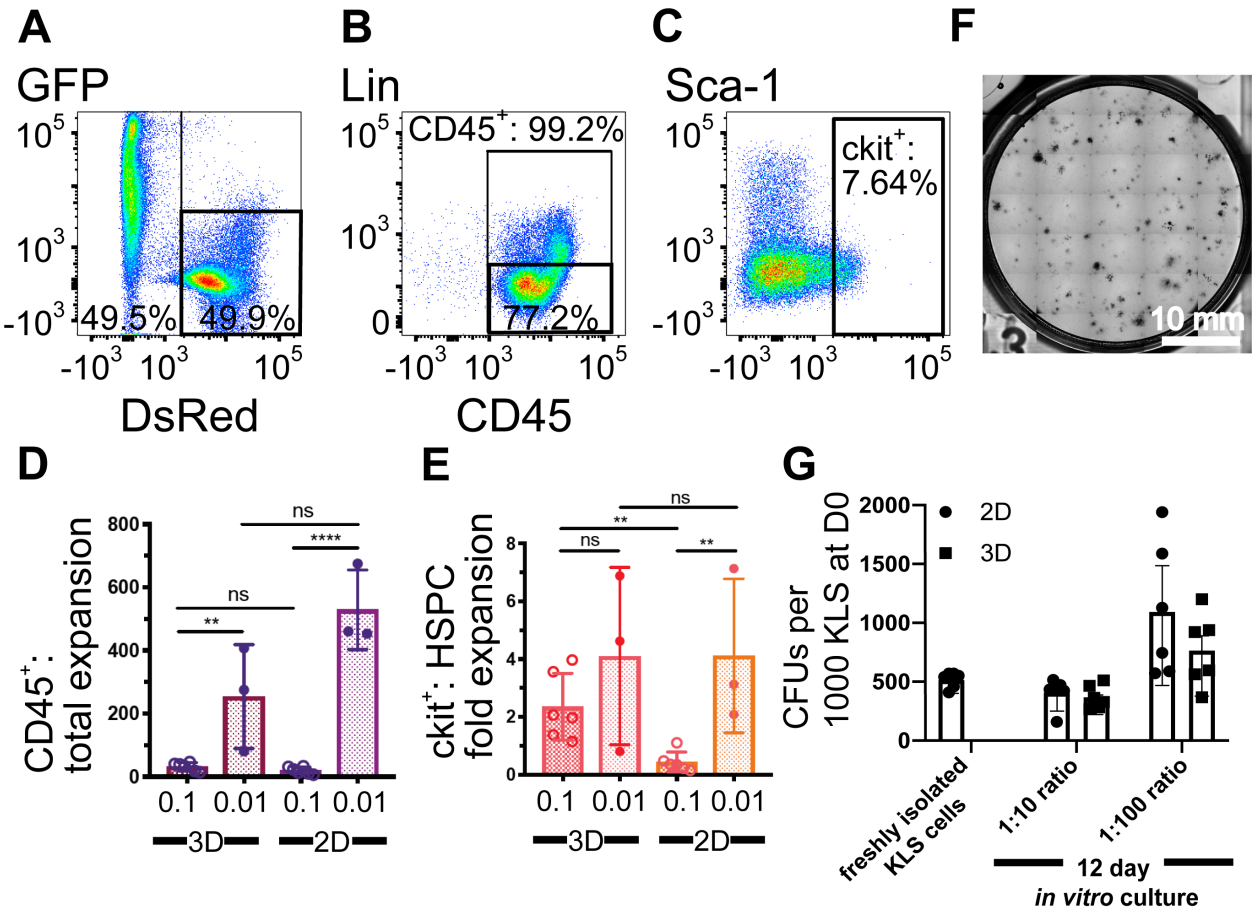

Fig. 3. 3D culture outcome compared to 2D controls via flow cytometry and colony forming assays.

(A-C) Example flow cytometry analysis gating (Coculture in CCM scaffolds, initial seeding density KLS:OP9=1:10, analysis at 12 days. After initial gating to live cells (low DAPI labeling due to intact membrane, isolation from counting beads, not shown), we performed a first gating using the intrinsic DsRed (HSPC and progeny) and GFP (OP9) expression **(A)**. The $DsRed^{+}GFP^{-}$ was further analyzed for Lineage and CD45 markers, allowing to isolate the Lin-CD45+ population **(B)**. The stem and progenitor fraction was finally obtained as $cKit^{+}$ cells within the Lin-CD45+ population **(C)**. **(D)** Total CD45+ expansion through flow cytometry, identifying 2D and 3D cell proliferation for both the 1:10 and 1:100 seeding densities. **(E)** Total CD45+, cKit+ cell expansion for the same conditions, demonstrating closer similarities between the four conditions. **(F)** Total colony count after 7 days in methylcellulose medium, after harvesting total cells from the CCMs (after 12 days of *in vitro* culture).

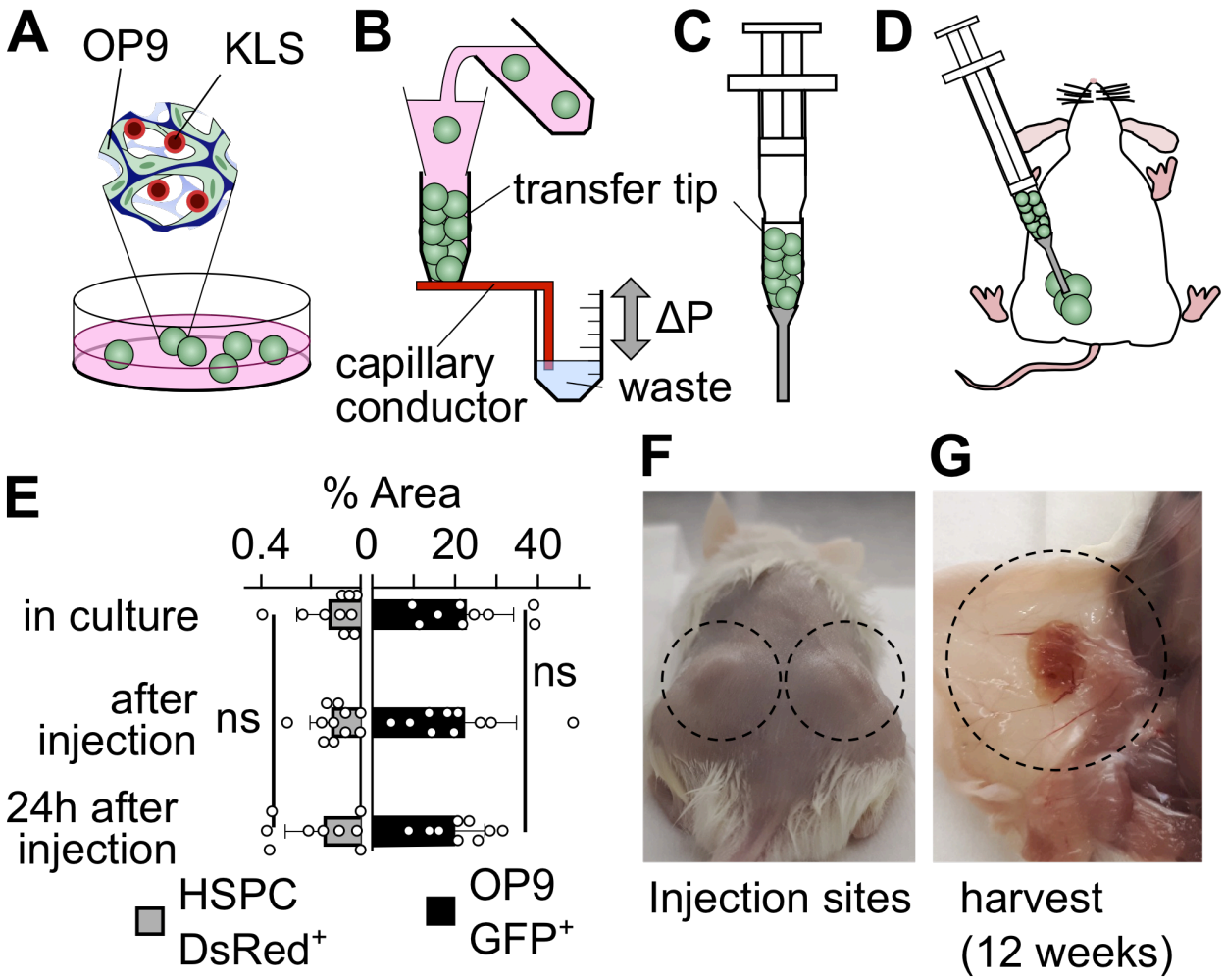

Fig. 4. Implantation of CCM-based co-cultures. (A) After seeding, the co-cultures can be cultured in-vitro as classical microcarrier suspension cultures. **(B)** To prepare an implant, the material is partially dehydrated to by equilibrating to a predefined hydrostatic pressure level (ΔP), typically on the order of 0.2kPa (ca. 2cm water column). This is done in a specifically designed transfer tip. **(C)** Once equilibrated and filled with implantable co-culture biomaterial, the transfer tip is attached to a syringe and an implantation catheter (to avoid accidental intravascular injection). **(D)** The co-culture biomaterial is injected subcutaneously. **(E)** *In vitro* assessment of injection viability as quantified through GFP+ OP9 MSC and HSPC cell confluence before, immediately after, and 24 hours after injection (biomaterial seeded 1:100 HSPC – OP9, used at day 1 *in vitro*). **(F)** Macroscopic external view of the implant in the subcutaneous dermal tissue 12-weeks post-implantation. **(G)** Visibly vascularized scaffold after sacrifice, seen from the inside of the skin flap.

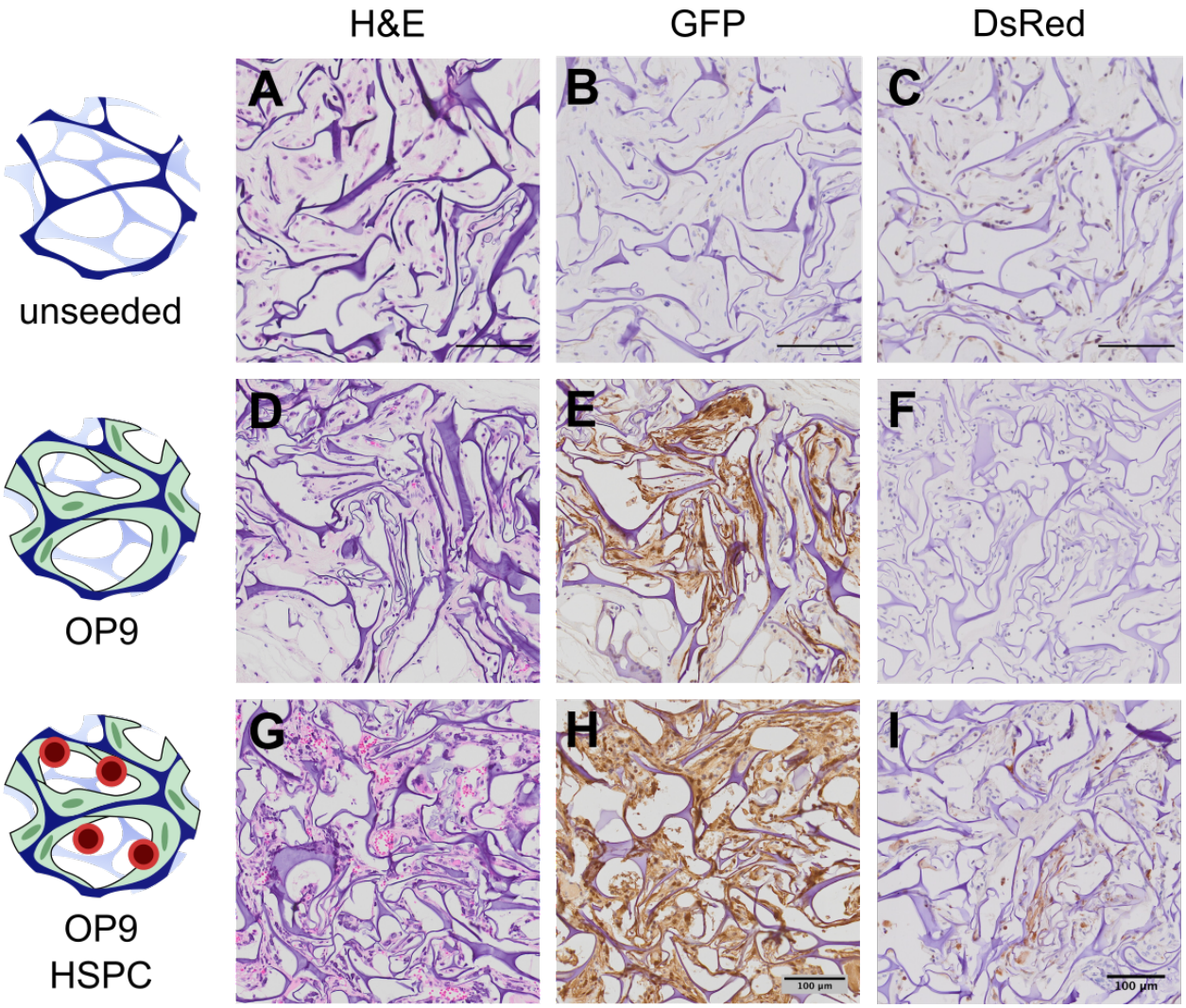

Fig. 5. Histology and cellular composition of implanted scaffolds.
Unseeded CCMs **(A-C)**, as well as CCMs cultured with OP9 **(D-F)** or with 1:10 "high" co-cultures of OP9 and KLS cells **(G-I)** were implanted into the dorsal skin of NSG mice, and retrieved after sacrifice at 12 weeks. Samples were processed for hematoxylin/eosin (H&E) staining **(A, D, G)**, as well as immunohistochemistry with primary antibodies directed against GFP (**B, E, H**, marker for OP9 cells) and DsRed (**C, F, I**, marker of HSPC and progeny).

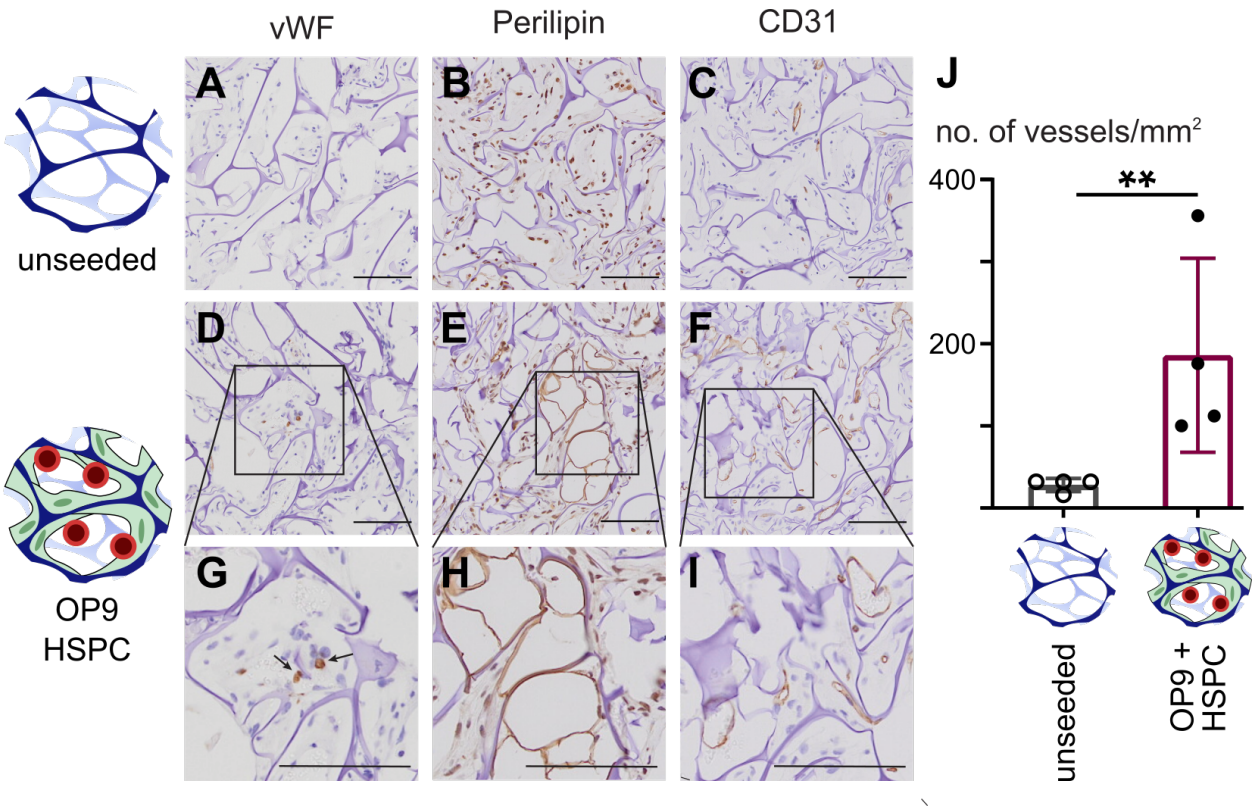

Fig. 6. Immunohistochemistry of scaffolds transplanted *in vivo*.
Unseeded scaffolds **(A-C)** and HSPC/OP9-seeded scaffolds **(D-I)** were recovered 12 weeks after subcutaneous transplant. Paraffin sections of scaffolds were stained with anti-vWF (**A, D, G,** arrows indicate megakaryocytes), anti-Perilipin (**B, E, H**), and anti-CD31 (**C, F, I**), and antibodies. Scale bars are 100µm. CD31+ vessels were quantified **(J)**, error bars indicate mean ±SD ($p<0.003$).

Supplementary Information List (separate file):

- **Supplementary 1: Uniaxial compression of scaffolds seeded with co-cultures**
- **Supplementary 2: Video file: Demonstration of drying device**
- **Supplementary 3: Drying device for CCM concentration**